

Dissecting the Cloud and Precipitation Microphysics with Cloud Dynamic Characteristics:

Complexity of Mesoscale Convective System

Sumit Kumar¹, Neelam Malap¹, Sachin Patade¹, Gayathri Kulkarni¹, Soumya Samanta¹, Resmi E A², Shivsai Ajit Dixit¹,

P Murugavel¹, and Thara Prabhakaran¹

¹ Indian Institute of Tropical Meteorology, Pune - 411008, India.

² National Centre for Earth Science Studies (NCESS), Thiruvananthapuram - 695011, Kerala, India.

Corresponding author email: sumit.chauhan@tropmet.res.in, sum8528@gmail.com



Abstract no. Th-2.01



IITM

BACKGROUND

- The Indian summer monsoon provides 70-80% of the annual rainfall across the Indian subcontinent, out of which ~30-40% of the rainfall is sourced from stratiform precipitation (Parthasarathy et al. 1994; Gadgil 2003; Rajeevan et al. 2013).
- The cloud systems consist of convective and stratiform precipitation regions with different dynamics and microphysics (Houze 1997; Pandey et al. 2014). The hydrometeor microphysics of the precipitation events in the monsoon environment is rarely examined using polarimetric radar and Weather Research and Forecasting (WRF) modeling.
- This study aims to address two key scientific questions: (1) How do microphysics and hydrometeor characteristics differ between stratiform and convective precipitation during mesoscale convective system (MCS), (2) How well do bin microphysical schemes in the WRF model simulate these observed characteristics and analyze the simulated hydrometeor uncertainty?
- To answer these questions, we utilize C-band polarimetric radar to investigate the characteristics of microphysics and hydrometeors from 15 to 16 August 2018.
- Additionally, we employed a Spectral Bin microphysical scheme within the WRF to simulate the rainfall event and analyze the simulated hydrometeors with radar observations.

DATA AND METHODOLOGY

- The present study explores the microphysics and hydrometeor features of the Mesoscale convective system identified using a C-band polarimetric radar in the summer monsoon of 2018 (15th to 16th August) over the southwest peninsular Indian region.
- Locations of the radar and the WRF domain configuration is presented along with the topography of the study area in Fig. 2.
- The details of the instruments installed at the observatory location and the data sets used are given in Table 1.
- Quality control measures for avoiding pixels where Z_h exceeds 70 dBZ or ρ_{hv} is less than 0.7 (Farr et al. 2007)
- The method by Steiner et al. (1995) has been adopted for the separation of convective from stratiform pixels, and an example of a PPI diagram of radar reflectivity is shown in Figure 1.
- We have implemented the HID methodology by Dolan et al. (2013) to investigate the hydrometeors during the monsoon phases. It determines the dominating hydrometeor type in a radar sample volume.

Fig. 1. (a) PPI diagrams of radar reflectivity averaged between 2.5 - 3.5 km height at 0806 IST on 16th Aug 2018, and (b) the identified convective (red) and stratiform (blue) regions.

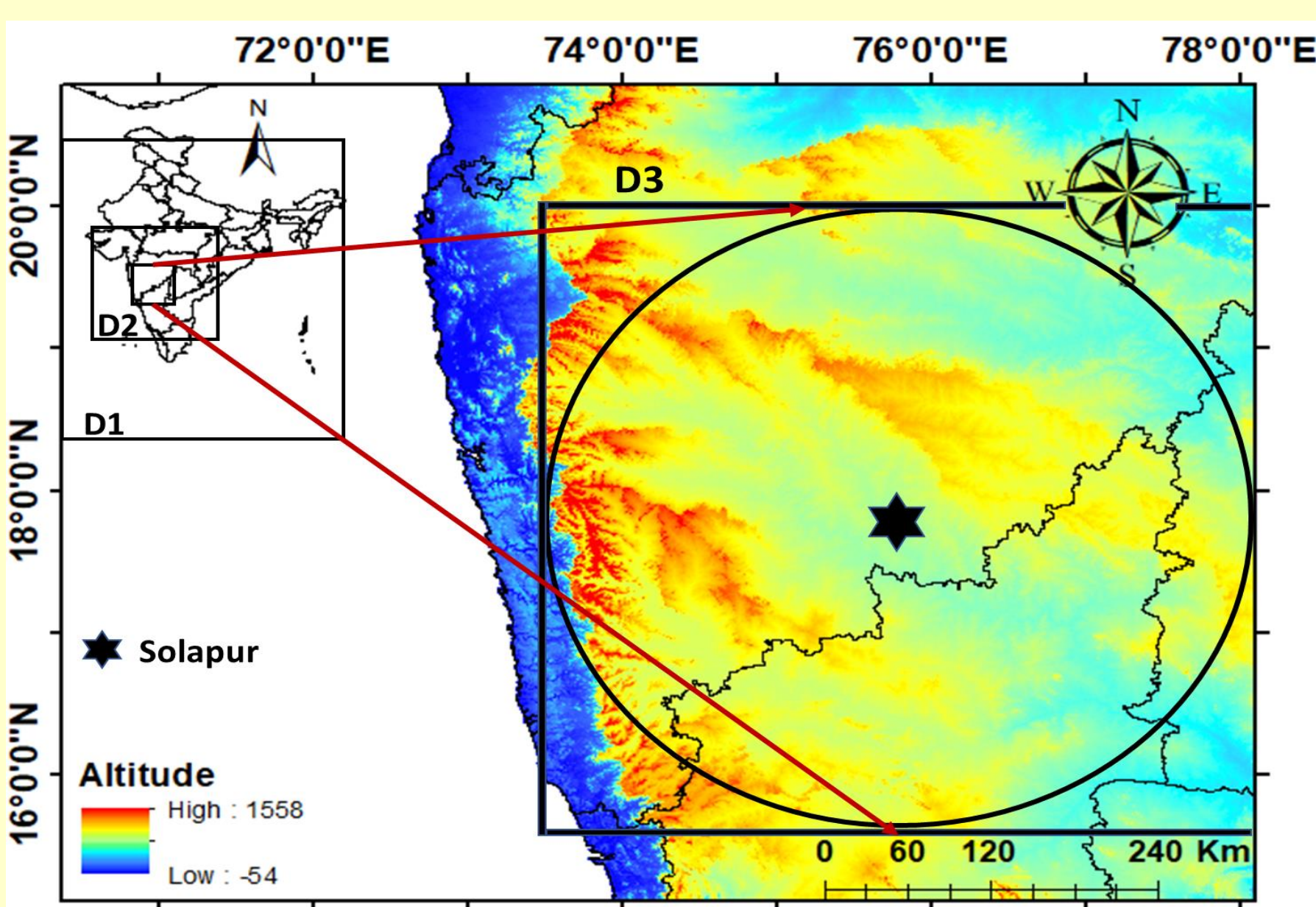
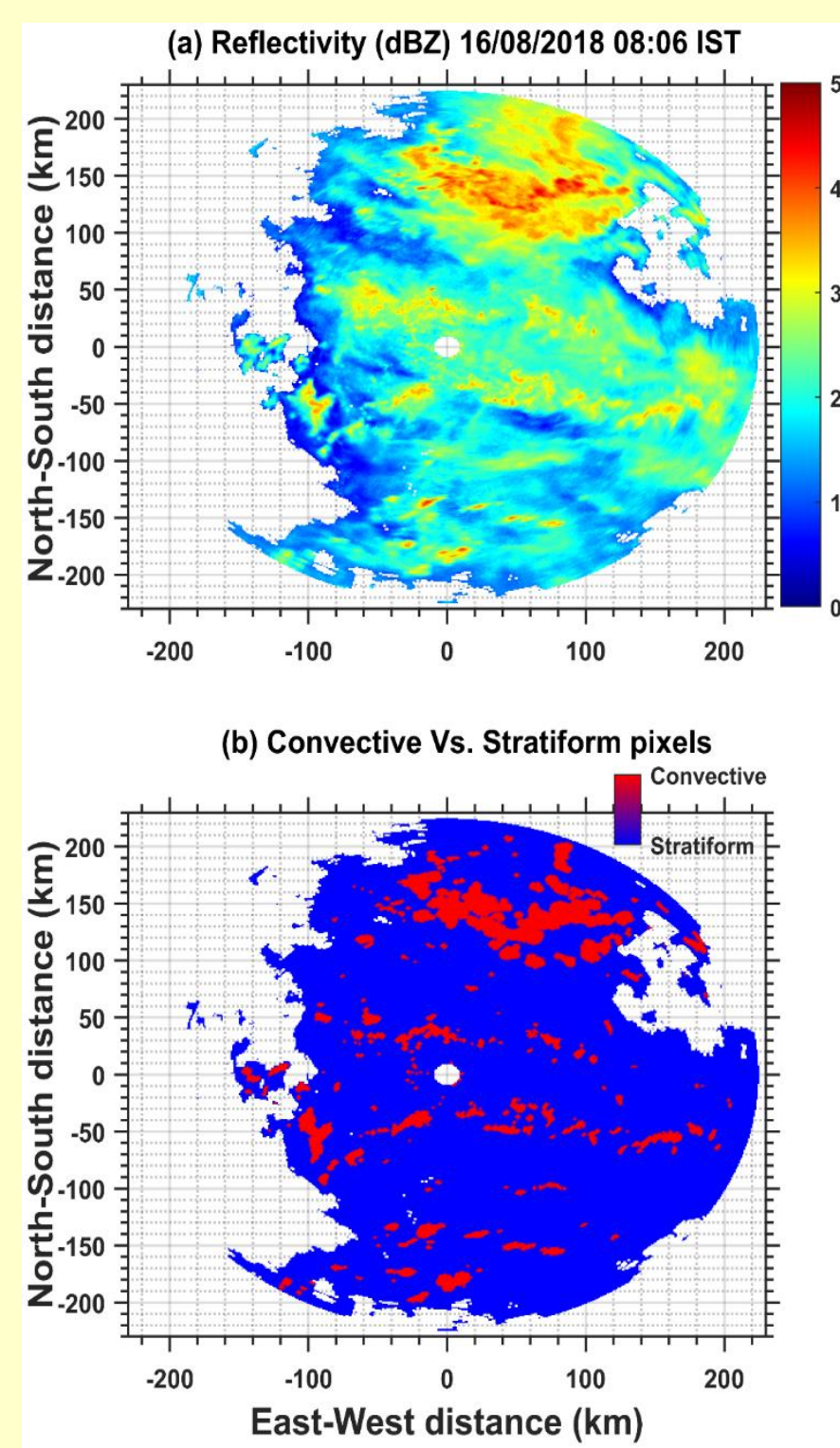


Fig. 2. The elevation map of the study area shows the radar region with a three-domain configuration of WRF simulations. The area of the map represents the domain D1 (02.53°S – 38.01°N, 54.59°–97.13°E) with horizontal grid intervals of 9 km. The area enclosed by the domain D2 (10.98°–24.50°, 68.77°–82.95°E) and domain D3 (15.49°–19.99°N, 73.50°–78.22°) grid intervals of 1 km. The circle in the D3 domain represents the radar's 250 km radii coverage.

Table 1 summarises various datasets and parameters that are used in this study.

Sl. No.	Data source	Parameters	Spatial resolution	Temporal resolution
1.	Polarimetric Doppler Weather Radar (C-band) C-band Polarimetric DWR (at Solapur)	Reflectivity at horizontal polarization (dBZ), differential reflectivity (dB), differential propagation phase (deg.), cross-correlation	150 m along the radial and 1° along azimuth	~15 min.
2.	Radiosonde (over Solapur)	Temperature profiling	In situ	-
3.	Radiometer	Temperature, humidity, liquid water, CAPE, and CIN profiling	Remote sensing	1 minute
4.	INSAT-3DR	Brightness temperature (K)	4 x 4 km	Hourly.
5.	ERA5 reanalysis	Zonal and Meridional Wind (m/s)	0.25° x 0.25°	Hourly.
6.	GPM	Precipitation	0.1° x 0.1°	Hourly.

ACKNOWLEDGEMENTS

The authors sincerely thank the Director, Indian Institute of Tropical Meteorology (IITM), Pune, for encouragement and support. IITM is funded by the Ministry of Earth Sciences (MoES), Govt. of India. The first author duly acknowledges the support from the 'HPC-Pratyush Support team' at IITM, Pune, for the model simulations.

RESULTS

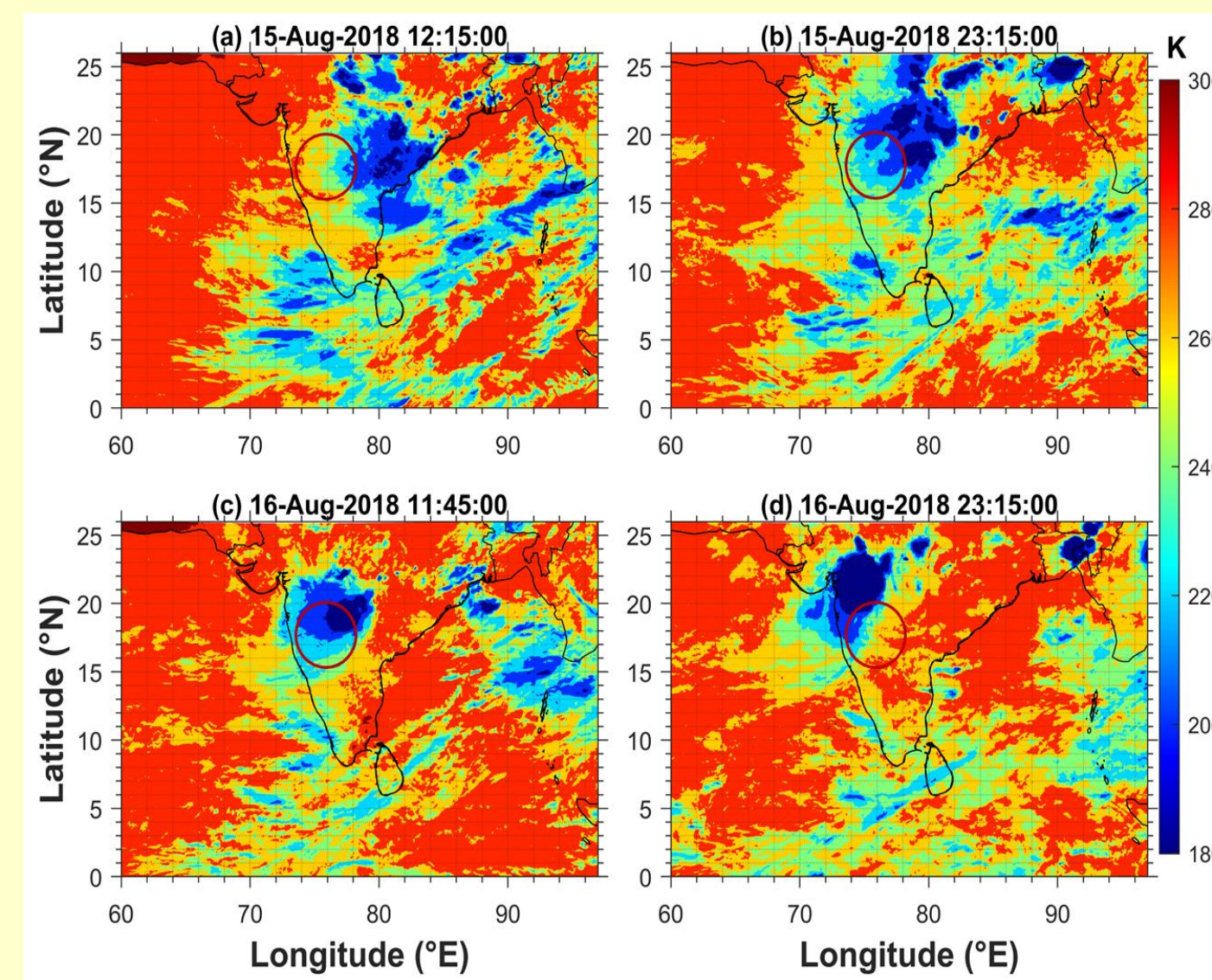


Fig. 3. The spatial distribution of brightness temperature (K) on 15th and 16th August 2018 over the Indian region (0-26°N, 65-97°E) using INSAT-3DR data.

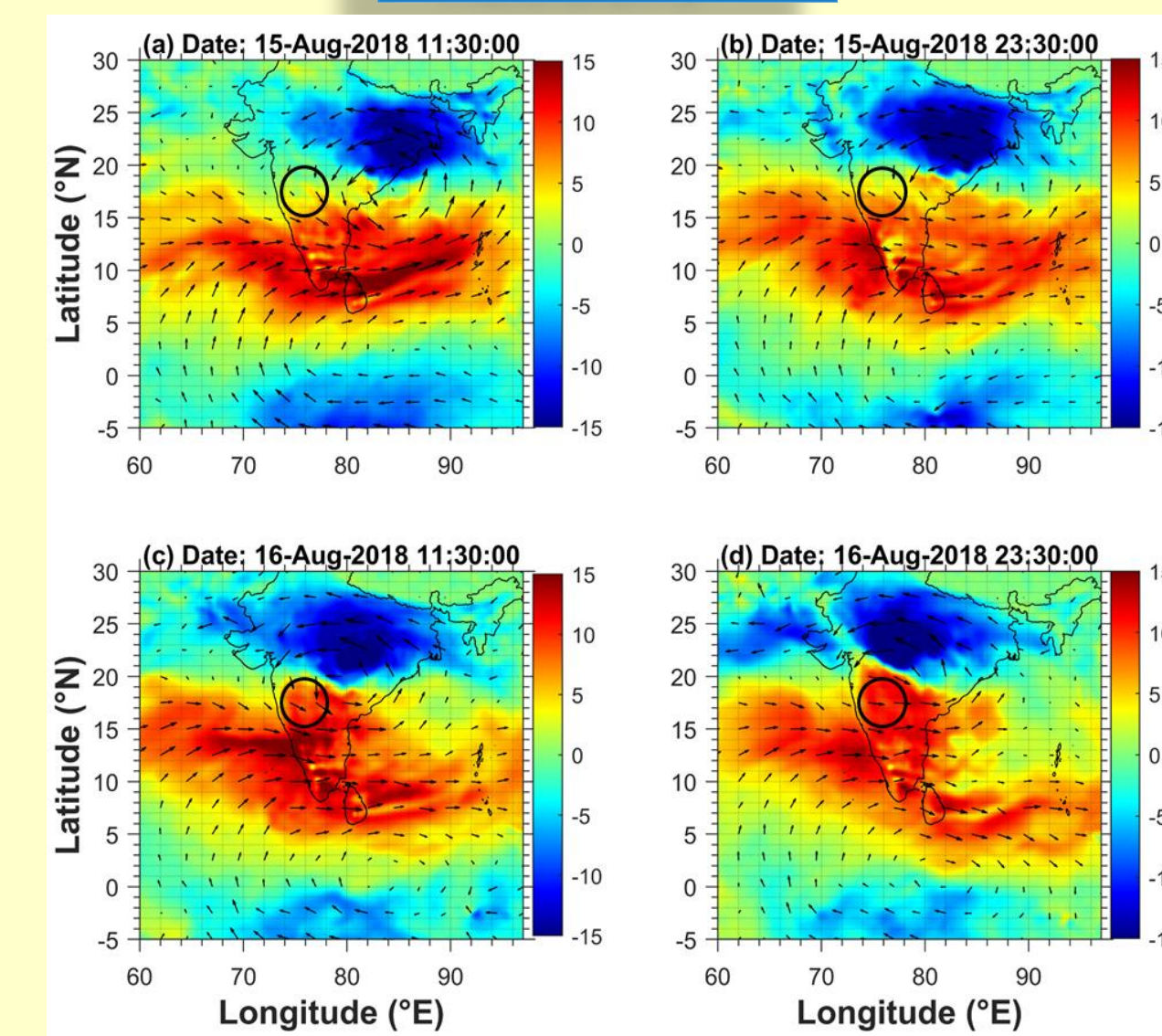


Fig. 4. The spatial distribution of zonal wind anomaly on 15th and 16th August 2018 over the Indian region from 0-26°N, 60-97°E at 850 hPa. The wind anomaly is calculated on the basis of the last 20 years (from 1998 to 2018) using ERA5 reanalysis data. The black circle represents the Solapur radar region.

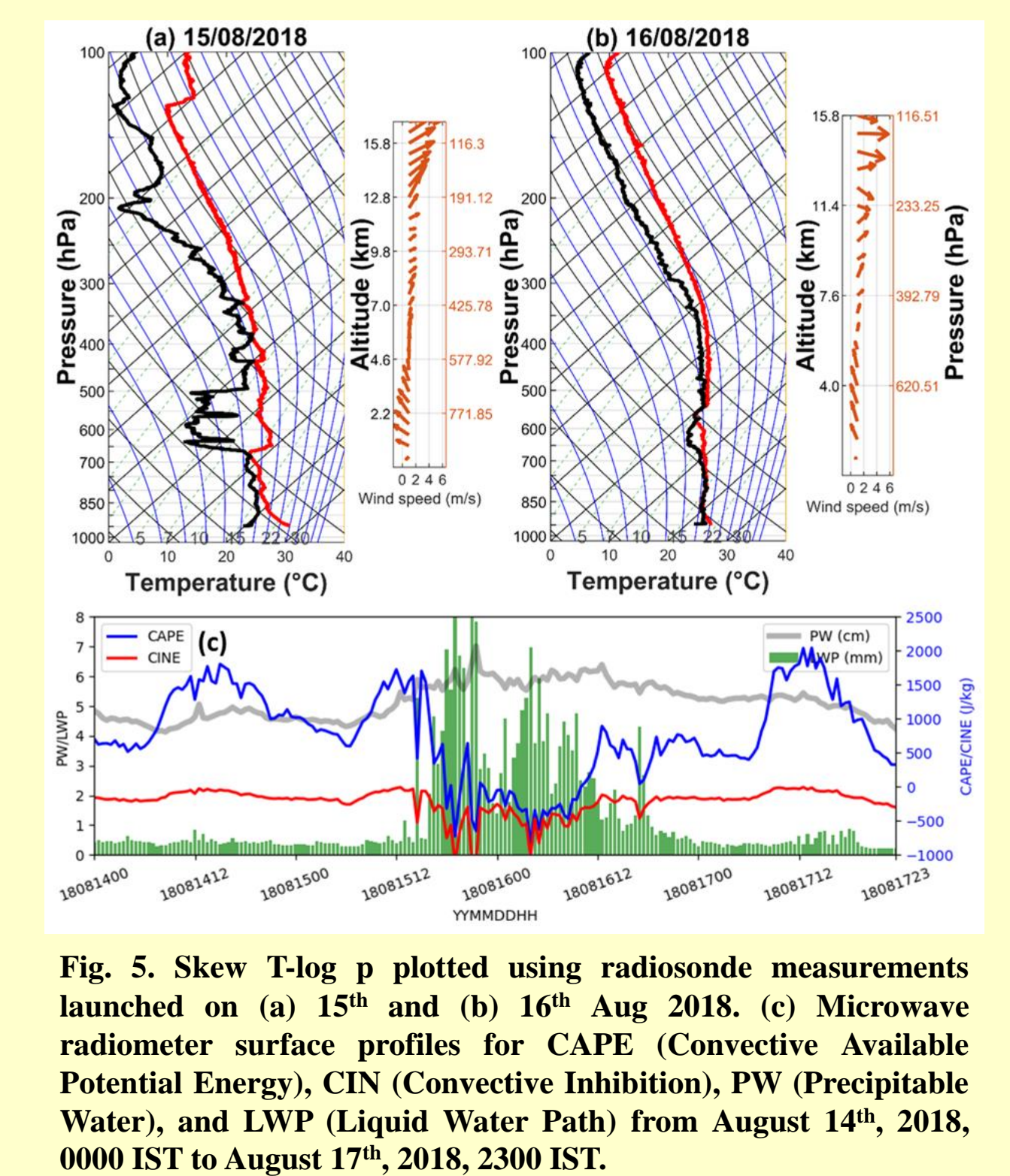


Fig. 5. Skew T-log p plotted using radiosonde measurements launched on (a) 15th and (b) 16th Aug 2018. (c) Microwave radiometer surface profiles for CAPE (Convective Available Potential Energy), CIN (Convective Inhibition), PW (Precipitable Water), and LWP (Liquid Water Path) from August 14th, 2018, 0000 IST to August 17th, 2018, 2300 IST.

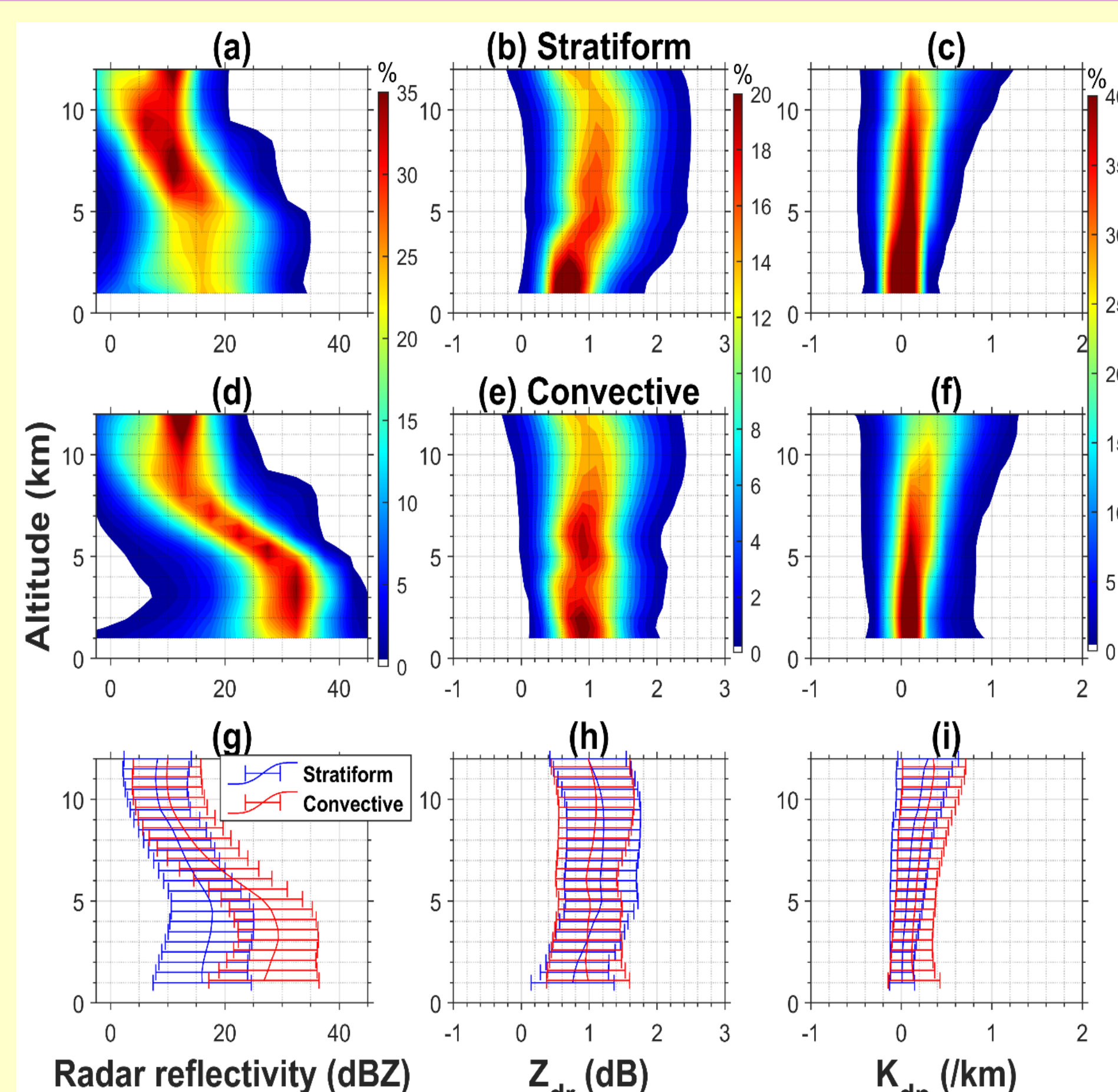


Fig. 6. Contour frequency by altitude diagram (CFAD) of Reflectivity, differential reflectivity (Z_{dr}), and specific differential phase (K_{dp}) for stratiform (d-f) and convective (a-c) regions. (g-i) Mean vertical profile with standard deviation bar bars of Z_h , Z_{dr} , and K_{dp} over stratiform (blue) and convective (red) regions.

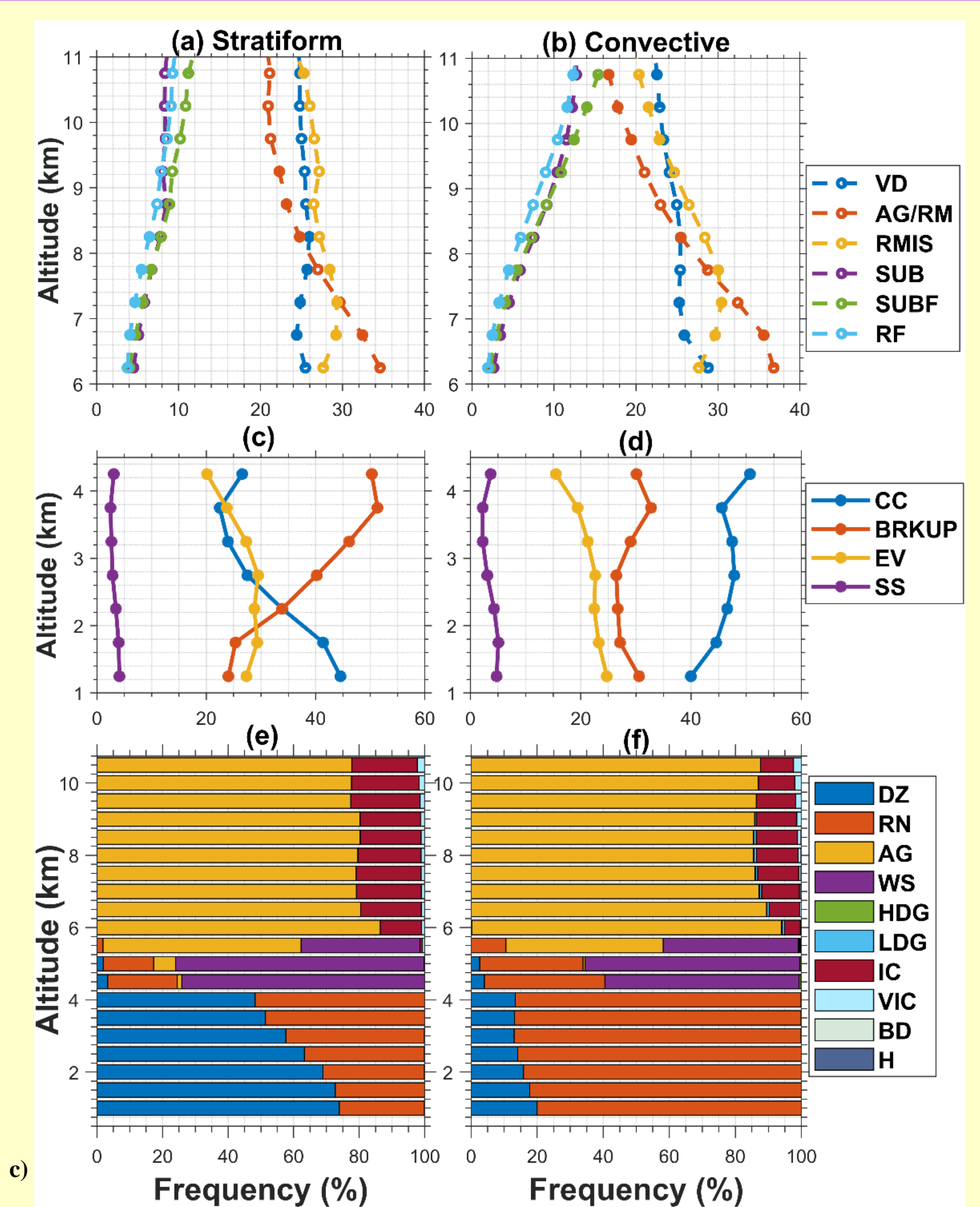


Fig. 7. Frequency altitude diagram of cloud and precipitation microphysics during (a & c) stratiform and (b & d) convective precipitation over the Solapur region from 00:00 IST, 15th Aug

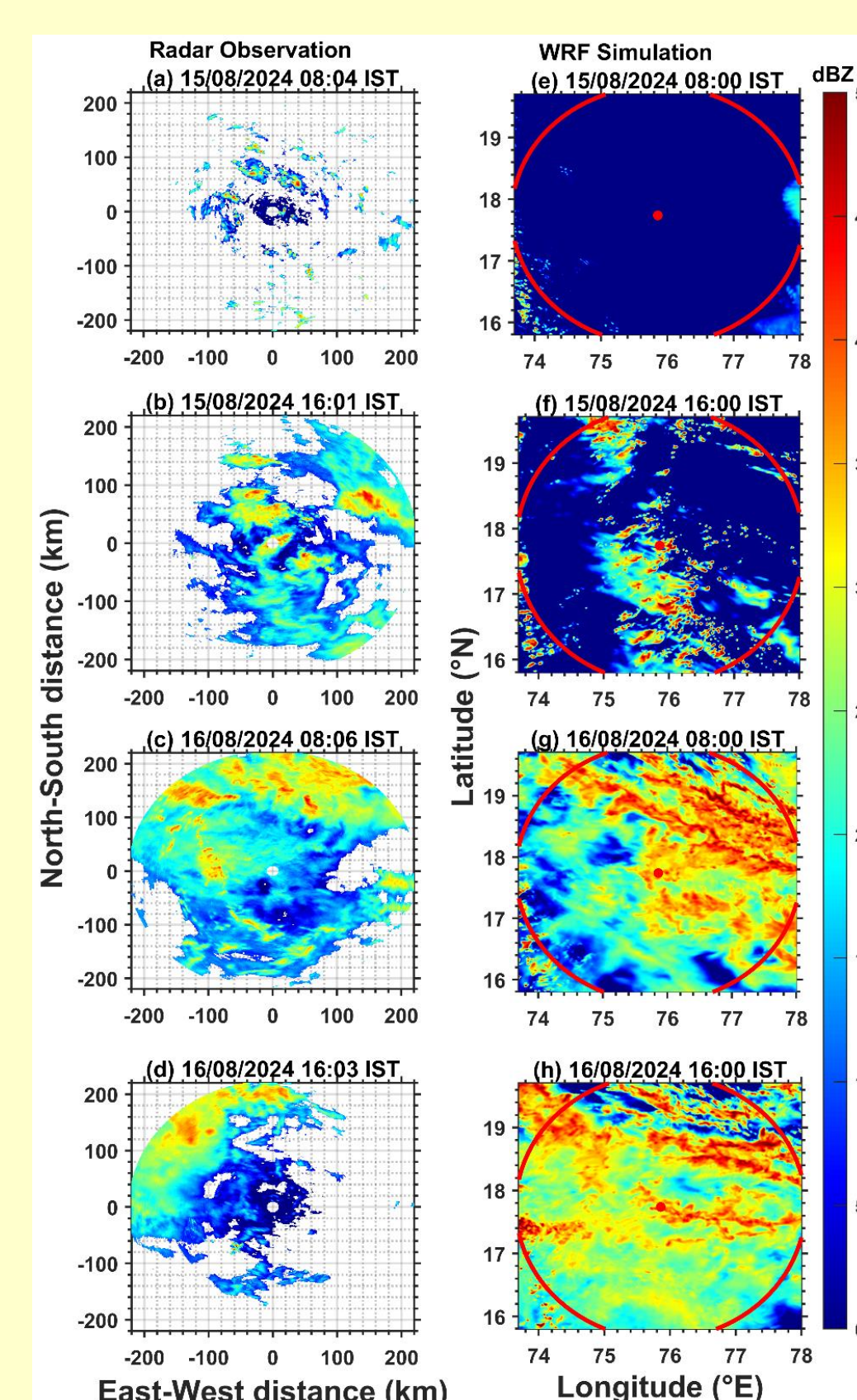


Fig. 8. PPI of (a-d) horizontal radar reflectivity (dBZ) from C-Band polarimetric Radar and (e-h) simulated radar reflectivity (dBZ) averaged between 2.5-3.5 km on 15th and 16th Aug 2018. The red circle in the right column defines the radar range over the simulated region.

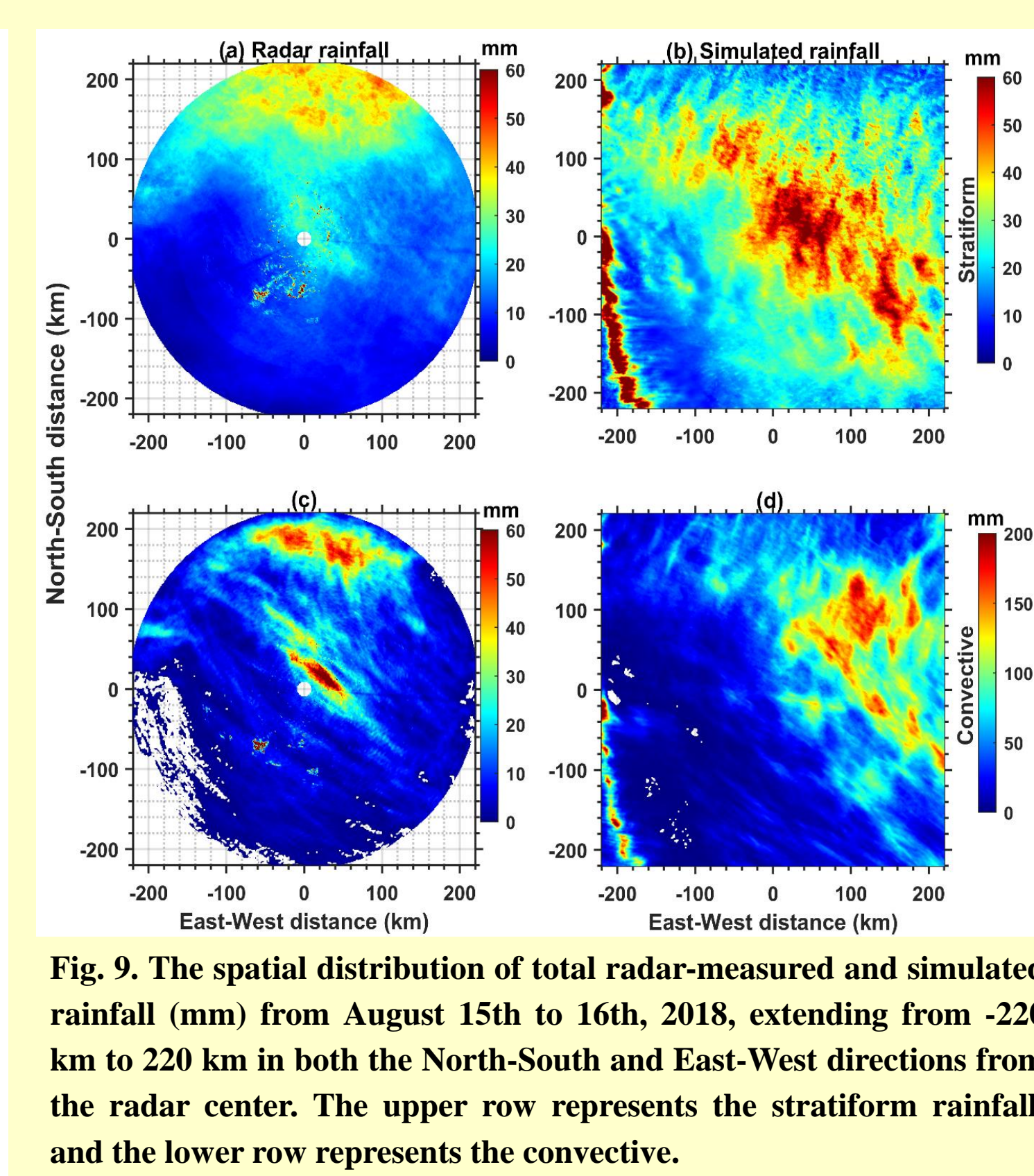


Fig. 9. The spatial distribution of total radar-measured and simulated rainfall (mm) from August 15th to 16th, 2018, extending from -220 km to 220 km in both the North-South and East-West directions from the radar center. The upper row represents the stratiform rainfall, and the lower row represents the convective.

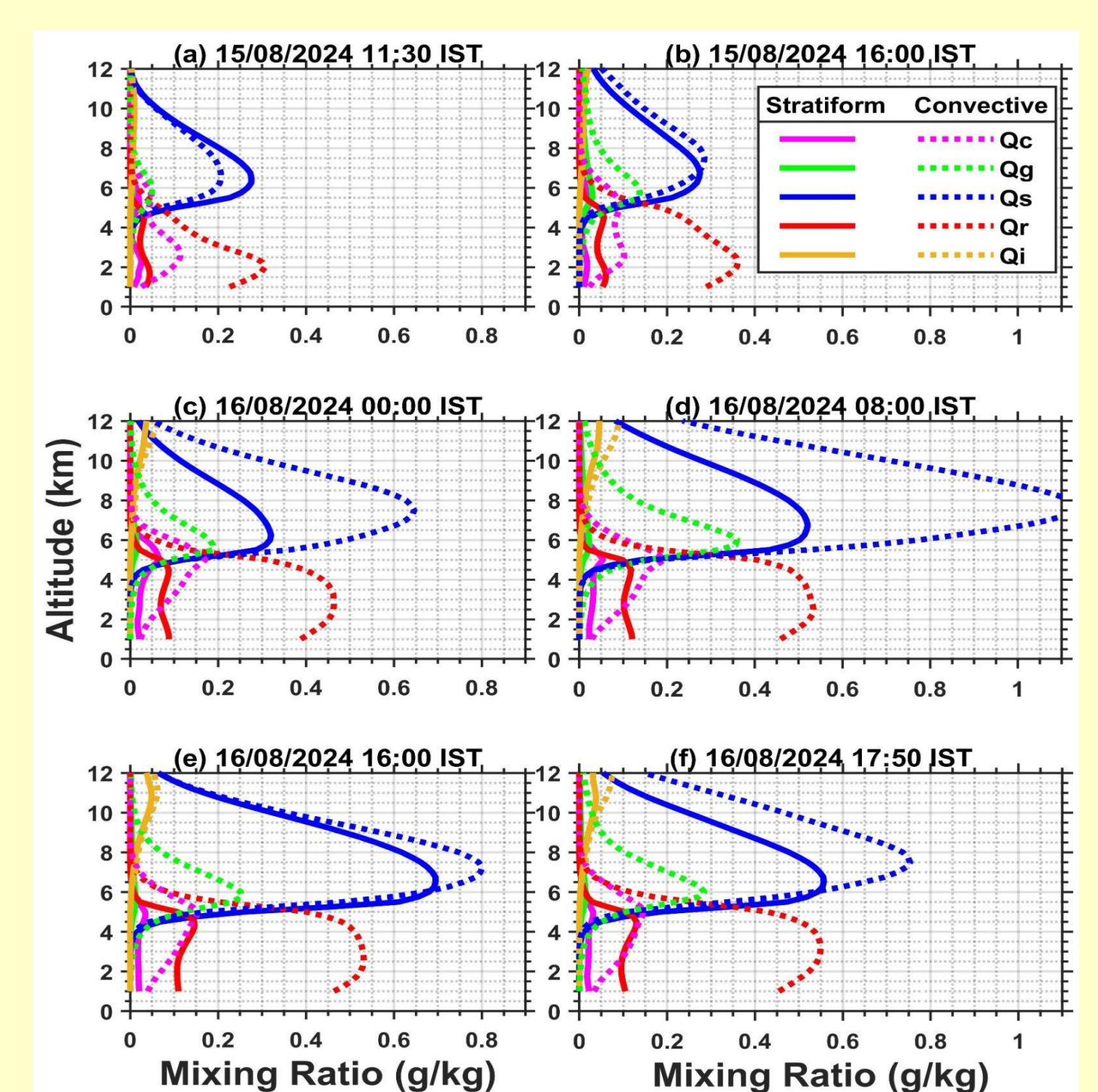


Fig. 10. Area average convective and stratiform mixing ratio (g/kg) over the Solapur region from WRF SBM-fast simulation on 15th and 16th October 2018.

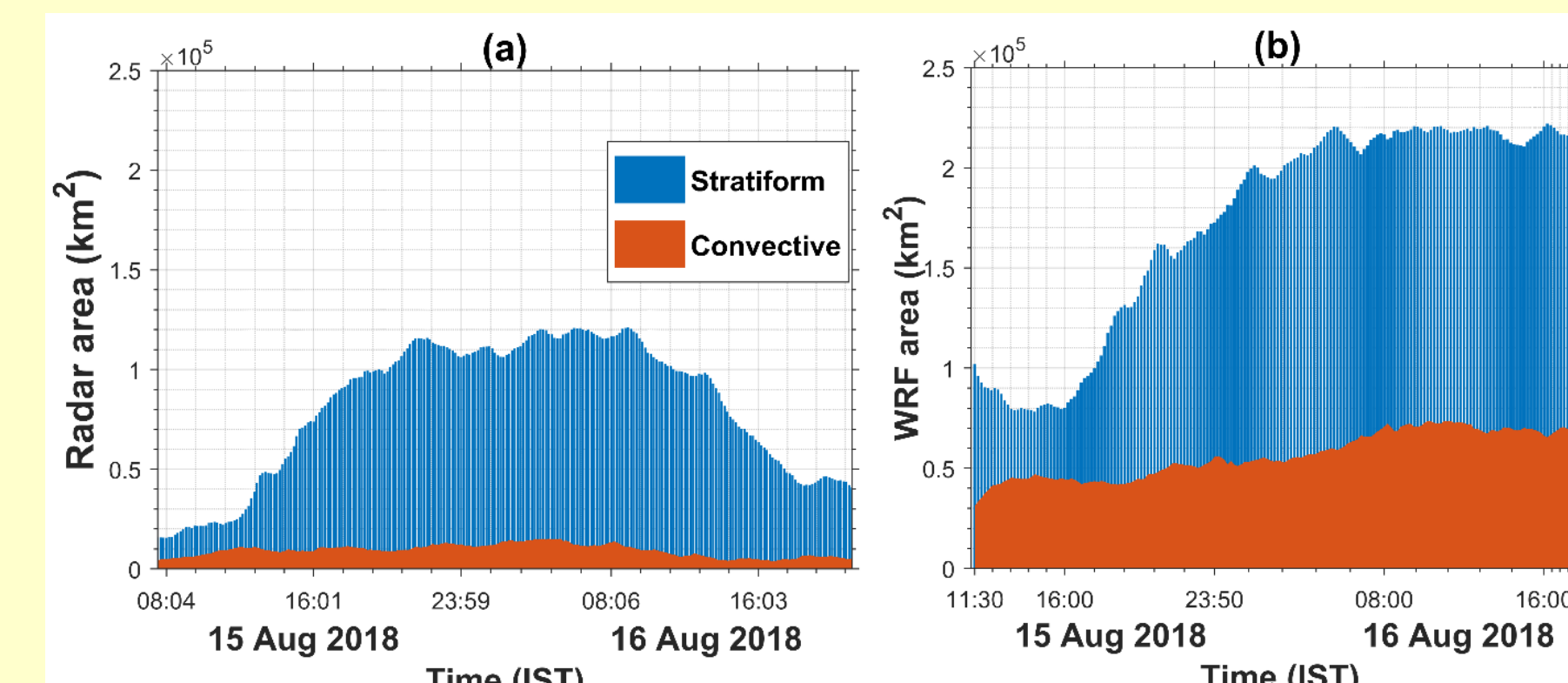


Fig. 11. (a) Time series of radar area (km^2) as stratiform (blue) and convective (red) precipitation region from 0800 IST, 15th Aug 2018 to 2000 IST, 16th Aug 2018. (b) Time series of the simulated area (km^2) as stratiform and convective precipitation region from 1130 IST, 16th Aug 2018 to 1800 IST, 16th Aug 2018.

CONCLUSIONS

- Convective regions show higher reflectivity (mean 30 dBZ, peaks >40 dBZ), indicating intense rainfall, while stratiform regions exhibit lower reflectivity (mean 17 dBZ, peaks 30 dBZ) and steady rain. Differential reflectivity (Z_{dr}) is stable (~-1 dB) in convective regions but decreases from 1.2 to 0.8 dB below the melting layer in stratiform areas.
- Radar observations reveal that 89.9% of the MCS region is stratiform precipitation, while the model estimates a lower proportion of 72.7%. During stratiform precipitation, breakup dominates between 4.25 km and 2 km, followed by collision-coalescence, increasing drizzle from 50% to 74%. In convective precipitation, collision-coalescence peaks below the melting layer but decreases below 3 km as breakup and evaporation reduce rain hydrometeors from 86% to 80% near the surface.
- Radar-derived precipitation indicates an even split between convective and stratiform processes, while simulations show convective rainfall exceeding stratiform over three times, highlighting gaps in precipitation modeling.
- During convection, ice crystals peak in frequency at around 8 km altitude, with a dominance of 15%. Light-density graupel is observed around 2-3%, extending up to 8 km altitude. In contrast, aggregate particles dominate during stratiform precipitation, accounting for up to 80%, while ice crystals make up about 20%, with their peak frequency occurring around 7.5 km altitude.
- Above the melting layer, stratiform precipitation involves vapor deposition (VD), aggregation/rimming (AG/RM), and riming with ice splintering (RMIS), consistent up to 8 km, with RMIS peaking at 7.25 km and VD minimizing at 6.75 km. In convective precipitation, RMIS peaks at 7.75 km, with AG/RM processes exhibiting higher growth than in stratiform regions.
- During convection, ice crystals peak at 8 km with a dominance of 15%, while light-density graupel (2-3%) extends to 8 km. In stratiform precipitation, aggregate particles dominate (~80%), with ice crystals (~20%) peaking at 7.5 km altitude. The C-band radar, coupled with fuzzy logic-based hydrometeor identification, effectively distinguishes between hydrometeor types in stratiform and convective processes. This differentiation is critical for refining quantitative precipitation estimation (QPE).
- Enhanced understanding of hydrometeor evolution and precipitation pathways in MCSs is essential for improving the representation of these systems in numerical weather prediction and climate models.